

Tailored Optical Polarization in Nano-Structured Metamaterials

Bernardo S. Mendoza

Department of Photonics, Centro de Investigaciones en Óptica, León, Guanajuato, México

W. Luis Mochán

*Instituto de Ciencias Físicas, Universidad Nacional Autónoma de México,
Apartado Postal 48-3, 62251 Cuernavaca, Morelos, México.*

A very efficient method for the calculation of the effective optical response of nano-structured composite systems allows the design of metamaterials tailored for specific optical polarization properties. We use our method to design 2D periodic arrays of sub-wavelength dielectric inclusions within nanometric supported metallic thin films which behave as either an almost perfect linearly dichroic system, as a controllable source of circular polarized light, as a system with a large circular dichroism, or as a circular polarizer. All of these systems may be tuned over a wide energy range.

PACS numbers:

I. INTRODUCTION

The calculation of the macroscopic electromagnetic response of binary composite materials made up of inclusions of an ordinary material within another has been explored since the nineteenth century.^{1–3} Techniques such as electron beam lithography have allowed the fabrication of nano-structured systems with inclusions of specific shapes.^{4,5} Similarly, ion milling techniques have produced high quality periodic patterns of holes of various shapes forming two-dimensional (2D) arrays.^{6,7} Therefore, it is possible to conceive and fabricate devices with novel and exotic macroscopic optical properties.⁸ For example, a negative refractive index has been predicted and observed⁹ for a periodic metamaterial consisting of a dielectric matrix with a periodic lattice of noble metal inclusions of trapezoidal shape.¹⁰ Devices based on other metamaterials have been proposed to manipulate the direction of propagation of electromagnetic waves and bend their trajectories and to focus light in sub-wavelength regions using flat lenses,⁸ produce electromagnetic cloaking^{11–13} and shielding.¹⁴ Furthermore, metamaterials built with conductors may display hyperbolic dispersion relations¹⁵ which yield singular densities of states. They also display plasmonic resonances which may be used to guide electromagnetic energy¹⁶ in directions that may be controlled through the polarization of light.¹⁷ Chiral plasmonic metamaterials¹⁸ have been proposed to detect circularly polarized light.¹⁹ Thus, the development of fast computational procedures for efficiently obtaining the electromagnetic properties of new nano-structured systems has become very important.

In Ref. 20 we employed a scheme based on Haydock's recursive method²¹ and developed in Refs. 22 and 23 to obtain within the long-wavelength approximation the optical properties of systems with arbitrary geometry and composition. Among other applications, we studied a film made of a square lattice of dielectric elliptical cylinders and rectangular prisms within a conducting matrix. We obtained a strong birefringent and dichroic response, such as a range of frequencies for which rotating by 90° the angle of polarization of the incoming light could change the film from from being an almost perfect reflector to being an almost perfect absorber. The frequency where this behavior was displayed was easily tuned by geometrical modifications such as rotating the base of the prisms or the axes of the ellipses.

The tremendous speed improvement over other equivalent approaches such as that of Ref. 24 allows calculations for 2D²³ and 3D²² structures of arbitrary geometry, including interpenetrated inclusions, and allowing for dispersive and dissipative components. That approach is based on a local field effect theory²⁵ which incorporates into the macroscopic response the spatial fluctuations of the microscopic electric field due to the texture of the composite. Similar homogenization procedures are also found in Refs. 24,26–29. Our calculations proceeded from digitized images of the system, such as a photograph or a drawing, which can be manipulated by standard software to explore the influence of geometry on response. This allowed us to obtain artificial materials with the sought optical properties. As long as we consider only sub-wavelength lengthscales, we cannot explore effects such as geometrically induced chirality^{18,30–32} or magnetism in left-handed metamaterials, although we have developed a generalization³³ of our recursive procedure^{22,23} and we have shown that a macroscopic approach can deal with lengthscales comparable to wavelength and yield, for example, the photonic band structure of the system.

In this paper we explore the polarization acquired by light at anisotropic thin films of metamaterials, where we use this term to describe nano-structured composites whose properties differ from those of the natural materials of which it is manufactured. In a periodic composite we could expect two origins for an anisotropic behavior, even when the component materials are isotropic. One is due to the periodic lattice and another due to the shape of the

individual inclusions. Consider an inclusion with a shape that has well defined symmetry axes. If these coincide with the crystalline axes, they would also coincide with the principal axes of the macroscopic response. If however, the inclusions are rotated with respect to the crystalline lattice,³⁴ the principal axes of the macroscopic response would also *rotate* to new directions that in general will depend on the composition of the metamaterial and the frequency of the light, i.e., they will not be geometrically defined. Something similar would occur if the inclusions lack symmetry axes. Furthermore, if one or both of the components of the metamaterial are dissipative, then the principal directions are given by complex vectors and the corresponding normal modes would be in general elliptically polarized. In this paper we explore the polarization acquired by light as it is reflected by or transmitted through a thin film of a metamaterial made up of a dissipative metal with dispersionless dielectric inclusions with a simple shape that is not necessarily aligned with the crystalline axes.

We obtained nano-structured metamaterial films which display extreme linear dichroism and that mimic quarter wave plates that allow the conversion of linear to circular polarization, as well as optimized structures that yield a large circular dichroism and that produce circular polarized light when illuminated with unpolarized light, and these properties may be tuned over a wide tunable energy range.

The article is organized as follows. In Sec. II we briefly present the theoretical approach used for the calculation of the macroscopic dielectric response of the metamaterial, to describe the elliptical polarization of the fields and normal modes and to calculate the optical properties of the metamaterial. In Sec. III we present results for two-dimensional periodic structures with inclusions of different shapes and orientations. Finally, in Sec. IV, we present our conclusions.

II. THEORY

A. Macroscopic response

In this subsection we review the main theoretical steps in order to calculate the macroscopic dielectric tensor, ϵ_M^{ij} following Refs. 22 and 23. We consider inclusions (B) embedded within a homogeneous material (A) forming a 2D periodic lattice in the $X - Y$ plane as shown, for example, in Fig. 1. The inclusions are taken to be generalized *cylinders* with an arbitrary cross section and translationally invariant along the Z axis. We assume that each region A or B has a well defined dielectric function ϵ_γ , where $\gamma = a, b$, which we assume local and isotropic, and that the cross section of the inclusions and the lattice periodicity are much smaller the free wavelength of light $\lambda_0 = 2\pi c/\omega$ with c the speed of light in vacuum and ω the frequency. For visible and near-infrared light, this implies that the inclusions must be of nanometric size.

The *microscopic* response is then described by

$$\epsilon(\mathbf{r}) = \epsilon_a - B(\mathbf{r})\epsilon_{ab} \quad (1)$$

where $\epsilon_{ab} \equiv \epsilon_a - \epsilon_b$ and $B(\mathbf{r})$ is the periodic characteristic function for the B regions; $B(\mathbf{r}) = 1$ when \mathbf{r} lies within the B regions and $B(\mathbf{r}) = 0$ when \mathbf{r} lies within the A regions. The characteristic function is periodic $B(\mathbf{r}) = B(\mathbf{r} + \mathbf{R})$, with $\{\mathbf{R}\}$ the Bravais lattice of the metamaterial.

According to Eq. (6) of Ref. 22 the inverse macroscopic longitudinal dielectric response of the system, defined through $\mathbf{E}_{ML} = \epsilon_{ML}^{-1} \cdot \mathbf{D}_{ML}$, is given by

$$\epsilon_{ML}^{-1} = \hat{\mathbf{q}}\eta_{00}^{-1}\hat{\mathbf{q}} = \hat{\mathbf{q}}\xi\hat{\mathbf{q}}, \quad (2)$$

where

$$\xi \equiv \eta_{00}^{-1} \quad (3)$$

is the 00 component of the inverse of the matrix

$$\eta_{\mathbf{G}\mathbf{G}'} \equiv \hat{\mathbf{G}} \cdot (\epsilon_{\mathbf{G}\mathbf{G}'} \hat{\mathbf{G}}'). \quad (4)$$

Here, \mathbf{E}_{ML} and \mathbf{D}_{ML} are the longitudinal projections of the macroscopic electric and displacement fields with wavevector \mathbf{q} , $\epsilon_{\mathbf{G}\mathbf{G}}$ is the Fourier transform of the microscopic dielectric response (Eq. (1)) with wave-vector $\mathbf{G} = \mathbf{G}'$, and $\{\mathbf{G}\}$ is the reciprocal lattice of the system, so that the microscopic constitutive equation may be written in reciprocal space as

$$\mathbf{D}_{\mathbf{G}}(\mathbf{q}) = \sum_{\mathbf{G}'} \epsilon_{\mathbf{G}\mathbf{G}'} \mathbf{E}_{\mathbf{G}'}(\mathbf{q}), \quad (5)$$

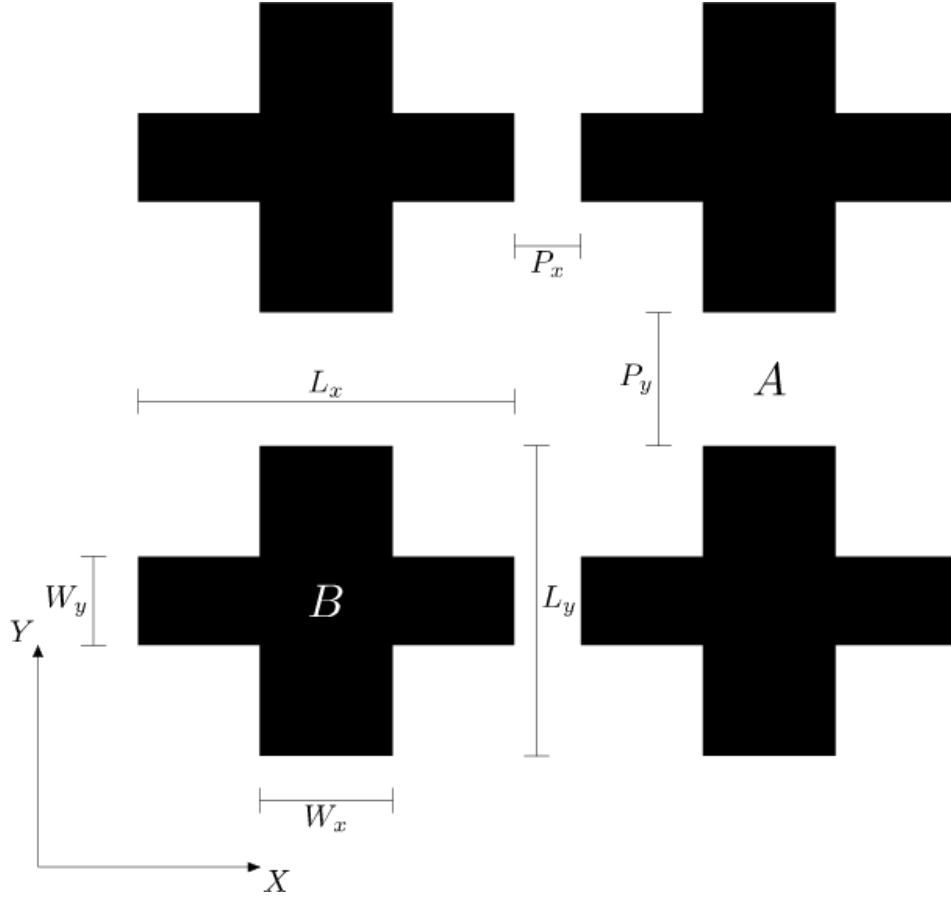


FIG. 1: Geometry of a metamaterial made up of cross shaped holes in a supported conducting film. We indicate the $X - Y$ axes, the length (L_x, L_y) of the beams, their width (W_y, W_x) and the widths of the conducting paths (P_x, P_y) between neighbor conducting rectangles. The crosses may additionally be rotated by an angle ϕ (not shown).

where $\mathbf{D}_{\mathbf{G}}(\mathbf{q})$ and $\mathbf{E}_{\mathbf{G}}(\mathbf{q})$ are the Fourier coefficients of the fields with wavevectors $\mathbf{q} + \mathbf{G}$. The wavevector \mathbf{q} of the macroscopic field may be interpreted as the conserved Bloch's vector. For succinctness, and in accordance to the long wavelength approximation, we have denoted the unit vectors $(\mathbf{q} + \mathbf{G})/|\mathbf{q} + \mathbf{G}|$ simply by $\hat{\mathbf{G}}$, and in particular, $\hat{\mathbf{0}} \equiv \mathbf{q}/q = \hat{\mathbf{q}}$.

We should emphasize that ξ and ϵ_{ML}^{-1} in Eq. (2) depend in general on the direction $\hat{\mathbf{q}}$ of \mathbf{q} . Nevertheless,

$$\epsilon_{ML} = \hat{\mathbf{q}} \xi^{-1} \hat{\mathbf{q}} = \hat{\mathbf{q}} \hat{\mathbf{q}} \cdot \epsilon_M \cdot \hat{\mathbf{q}} \hat{\mathbf{q}}. \quad (6)$$

is simply the longitudinal projection of the macroscopic dielectric tensor ϵ_M , and ϵ_M is independent of the direction $\hat{\mathbf{q}}$ in the long wavelength limit $\mathbf{q} \rightarrow 0$. Therefore, calculating $\xi(\hat{\mathbf{q}})$, for several propagation directions $\hat{\mathbf{q}}$, we may obtain *all* the components of the long-wavelength dielectric tensor $\epsilon_M(0)$.³⁵ For example, setting \mathbf{q} along $\hat{\mathbf{x}}$, Eq. (6) allows us to identify $\xi^{-1}(\hat{\mathbf{x}}) = \epsilon_M^{xx}$. Similarly, setting \mathbf{q} along $\hat{\mathbf{y}}$ we obtain $\xi^{-1}(\hat{\mathbf{y}}) = \epsilon_M^{yy}$, and setting \mathbf{q} along $\hat{\mathbf{x}} + \hat{\mathbf{y}}$ we obtain $\xi^{-1}((\hat{\mathbf{x}} + \hat{\mathbf{y}})/\sqrt{2}) = (\epsilon_M^{xx} + 2\epsilon_M^{xy} + \epsilon_M^{yy})/2$ from which we finally obtain $\epsilon_M^{xy} (= \epsilon_M^{yx})$ and thus, the full *transverse* dielectric tensor for waves propagating along the Z axis.

We can calculate ξ , appearing in Eq. (2), very efficiently using Haydock's recursion method, as shown in Refs. 22 and 23,

$$\xi = \frac{u}{\epsilon_a} \frac{1}{u - a_0 - \frac{b_1^2}{u - a_1 - \frac{b_2^2}{u - a_2 - \frac{b_3^2}{\ddots}}}}}, \quad (7)$$

where a_n and b_n are Haydock's coefficients, defined through

$$|\tilde{n}\rangle = \hat{\mathcal{H}}|n-1\rangle = b_{n-1}|n-2\rangle + a_{n-1}|n-1\rangle + b_n|n\rangle. \quad (8)$$

From Eqs. (3) and (4), ξ plays the role of a Green's function projected onto the macroscopic *state* $|0\rangle$ corresponding to a longitudinal plane wave with wave vector \mathbf{q} , the *spectral variable* $u(\omega) \equiv (1 - \epsilon_b(\omega)/\epsilon_a(\omega))^{-1}$ plays the role of a (complex) *energy* and

$$\mathcal{H}_{\mathbf{G}\mathbf{G}'} \equiv B_{\mathbf{G}\mathbf{G}'}^{LL} = \hat{\mathbf{G}} \cdot (B_{\mathbf{G}\mathbf{G}'} \hat{\mathbf{G}}') \quad (9)$$

plays the role of a Hamiltonian, with

$$B_{\mathbf{G}\mathbf{G}'} \equiv B_{\mathbf{G}-\mathbf{G}'} = \frac{1}{\Omega} \int d^3r B(\mathbf{r}) e^{-i(\mathbf{G}-\mathbf{G}') \cdot \mathbf{r}} = \frac{1}{\Omega} \int_v d^3r e^{-i(\mathbf{G}-\mathbf{G}') \cdot \mathbf{r}} \quad (10)$$

the Fourier transform of the characteristic function describing the geometry of inclusions which occupy the volume v within a unit cell of volume Ω . The recursion (8) starts from the macroscopic state $|0\rangle$ and we impose the orthonormality condition $\langle n|m \rangle = \delta_{nm}$, where δ_{nm} is Kronecker's delta function, to obtain the coefficients $a_{n-1} = \langle n-1|\tilde{n} \rangle = \langle n-1|\hat{\mathcal{H}}|n-1 \rangle$ and $b_n^2 = \langle \tilde{n}|\tilde{n} \rangle - a_{n-1}^2 - b_{n-1}^2$. After calculating the macroscopic response from Eq. (6) with different directions $\hat{\mathbf{q}}$, optical properties such as reflectance and absorptance may be calculated using standard formulae.^{36,37} Further details of this calculation in the 2D and 3D case may be found in Refs. 22 and 23, respectively.

For a generic system, all the Cartesian components of its macroscopic dielectric function ϵ_M^{ij} might be non-null, although some of the off-diagonal components ϵ_M^{ij} with $i \neq j$ might be zero due to the symmetries of the system. For the 2D metamaterials with translational symmetry along the Z axis that we study here, and for propagation along Z , ϵ_M^{ij} might be described by a complex 2×2 tensor

$$\epsilon_M = \begin{pmatrix} \epsilon_M^{xx} & \epsilon_M^{xy} \\ \epsilon_M^{yx} & \epsilon_M^{yy} \end{pmatrix}. \quad (11)$$

Here X and Y are the Cartesian directions in a coordinate system fixed to the unit cell (see Fig. 1). In general $\epsilon_M^{xx} \neq \epsilon_M^{yy}$ and $\epsilon_M^{xy} = \epsilon_M^{yx} \neq 0$. Thus, it is convenient to rotate the XY Cartesian system to the so called principal axes $X'Y'$ of the system in which $\epsilon_M^{i'j'}$ becomes diagonal. We note that the direction of the principal axes depend in general on the composition of the metamaterial and on the frequency, and are not completely determined by its geometry. Furthermore, since ϵ_M is in general complex due to the presence of dissipation, the vectors that define the principal axes are also complex. This means that their real parts could point in directions that differ from those of their imaginary parts, so that there are no *real* directions in space along which the fields of the corresponding eigenmodes oscillate. The polarizations of the eigenmodes are thus elliptical in general.

The eigenvalues λ_μ and eigenvectors \mathbf{V}_μ ($\mu = 1, 2$) of the 2×2 symmetric (though complex) tensor ϵ_M , are obtained straightforwardly.³⁸ Notice that as the macroscopic response is not in general a self-adjunct matrix, its eigenvectors are not orthogonal according to the Hermitian product. Nevertheless, in the nonretarded limit, the dielectric function is symmetric, so that its eigenvectors are orthogonal according to the Euclidean product. However, for convenience we normalize the eigenvectors using the Hermitian norm $\mathbf{V}_\mu^* \cdot \mathbf{V}_\mu = 1$ (otherwise, we would be unable to normalize the eigenvectors corresponding to circular polarization). The eigenvalues λ_μ correspond to the principal values of the macroscopic dielectric tensor ϵ_M , so the corresponding principal values of the complex index of refraction are

$$n_\mu = \sqrt{\lambda_\mu}. \quad (12)$$

B. Elliptical Polarization

To describe the polarization ellipse corresponding to the eigenvectors \mathbf{V}_μ , or more generally, to describe the polarization of an arbitrary monochromatic field $\mathcal{E}(t) = \text{Re}(\mathbf{E}_0 e^{-i\omega t})$ with frequency ω , we separate the complex amplitude \mathbf{E}_0 into real and imaginary parts

$$\mathbf{E}_0 = \mathbf{E}'_0 + i\mathbf{E}''_0, \quad (13)$$

to write

$$\mathcal{E}(t) = \mathbf{E}'_0 \cos(\omega t) + \mathbf{E}''_0 \sin(\omega t). \quad (14)$$

We interpret this real transverse vector equation as a 2×2 system of equations which we solve for $\sin \omega t$ and $\cos \omega t$. Then, we write the trigonometric identity $\cos^2(\omega t) + \sin^2(\omega t) = 1$ as the real quadratic form

$$\mathcal{E}^T(t) \cdot \mathcal{M} \cdot \mathcal{E}(t) = 1, \quad (15)$$

where we interpret $\mathcal{E}(t)$ as a column vector, $\mathcal{E}^T(t)$ as its transpose, and \mathcal{M} as a matrix with components

$$\mathcal{M}^{xx} = |E_{0y}|^2/D, \quad (16a)$$

$$\mathcal{M}^{xy} = \mathcal{M}^{yx} = -(E'_{0x}E'_{0y} + E''_{0x}E''_{0y})/D, \quad (16b)$$

$$\mathcal{M}^{yy} = |E_{0x}|^2/D, \quad (16c)$$

with

$$D = (E'_{0x}E''_{0y} - E'_{0y}E''_{0x})^2. \quad (17)$$

The quadratic equation (15) describes the polarization ellipse, which may be further characterized by diagonalizing \mathcal{M} , i.e., solving $\mathcal{M} \cdot \mathbf{v}_\pm = \Lambda_\pm \mathbf{v}_\pm$, to obtain the real positive eigenvalues Λ_\pm (choosing $\Lambda_+ \geq \Lambda_-$) and their corresponding eigenvectors \mathbf{v}_\pm . Writing $\mathcal{E}(t) = \mathcal{E}_+(t)\mathbf{v}_+ + \mathcal{E}_-(t)\mathbf{v}_-$ we obtain

$$\mathcal{E}^T(t) \cdot \mathcal{M} \cdot \mathcal{E}(t) = \Lambda_- \mathcal{E}_-^2(t) + \Lambda_+ \mathcal{E}_+^2(t) = 1, \quad (18)$$

which is the equation of an ellipse with major a and minor b semi-axes given by

$$a = \frac{1}{\sqrt{\Lambda_-}} \quad (19a)$$

$$b = \frac{1}{\sqrt{\Lambda_+}}. \quad (19b)$$

The angles α and β formed by the semi-axes a and b with respect to the X axis are given by

$$\tan \alpha = \frac{\Lambda_- - \mathcal{M}^{xx}}{\mathcal{M}^{xy}}, \quad (20a)$$

$$\tan \beta = \frac{\Lambda_+ - \mathcal{M}^{xx}}{\mathcal{M}^{xy}}. \quad (20b)$$

As expected, the minor and major semiaxes are mutually orthogonal.

The sense along which the field goes around the polarization ellipse is determined from the helicity $h = \text{sgn}[\hat{\mathbf{k}} \cdot \text{Re}(\mathbf{E}_0) \times \text{Im}(\mathbf{E}_0)]$, with $\hat{\mathbf{k}}$ a unit vector along the propagation direction. For waves moving along the positive Z axis,

$$h = \text{sgn}(E'_{0x}E''_{0y} - E'_{0y}E''_{0x}), \quad (21)$$

where $h = +1$ corresponds to right handed polarization \odot and $h = -1$ to left handed polarization \ominus . The degree of linearity or circularity of the polarization can be characterized through the so called *third flattening*, η of the polarization ellipses, defined through

$$\eta = \frac{a - b}{a + b}, \quad (22)$$

The values of η go from 1 for linear polarization to 0 for circular polarization, with intermediate values corresponding to elliptical polarization.

The analysis above may be applied to each of the normal modes of the macroscopic response of the metamaterial, as well as to the incoming, transmitted or reflected waves.

C. Thin Layer

Consider a monochromatic wave impinging normally from an isotropic transparent medium I into a film F of width d made of our metamaterial, from where it is partially reflected back into medium I and transmitted into a transparent isotropic medium T . Media I and T are characterized by their index of refraction n_i and n_t , while the film is characterized by the macroscopic tensor ϵ_M discussed in subsection II A. We can project the electric field \mathbf{E}_i of the incident wave into the principal *directions* of the response of the metamaterial

$$\mathbf{E}_i = \sum_{\mu} E_{i\mu} \mathbf{V}_{\mu} = \sum_{\mu} \mathbf{E}_i \cdot \tilde{\mathbf{V}}_{\mu} \mathbf{V}_{\mu}, \quad (23)$$

by introducing a dual basis

$$\tilde{\mathbf{V}}_\mu = \frac{\mathbf{V}_{\bar{\mu}}^\perp}{\mathbf{V}_\mu \cdot \mathbf{V}_{\bar{\mu}}^\perp}, \quad (24)$$

where for any possibly complex vector $\mathbf{v} = (v^x, v^y)$ on the XY plane we define $\mathbf{v}^\perp = (-v^y, v^x)$ as a perpendicular vector obtained by rotating clockwise by 90° on the plane, and where $\bar{\mu}$ denotes the index complementary to index μ , i.e., $\bar{1} = 2$ and $\bar{2} = 1$, so that $\tilde{\mathbf{V}}_\mu \cdot \mathbf{V}_\mu = 1$ and $\tilde{\mathbf{V}}_{\bar{\mu}} \cdot \mathbf{V}_\mu = 0$. Notice that the dual vectors are not necessarily *orthonormal* according to neither the Euclidean nor the Hermitian scalar product.

Each of the principal polarizations is conserved as the wave propagates along the system, and for each of them the film has a well defined index of refraction n_μ (Eq. (12)). Thus, we can obtain the optical properties of the system using the standard formulae for the reflection and transmission amplitudes of a thin film,³⁷ i.e.

$$r_\mu = \frac{r_{i\mu} + r_{\mu t} e^{2ik_\mu d}}{1 + r_{i\mu} r_{\mu t} e^{2ik_\mu d}} \quad (25a)$$

$$t_\mu = \frac{t_{i\mu} t_{\mu t} e^{ik_\mu d}}{1 + r_{i\mu} r_{\mu t} e^{2ik_\mu d}}, \quad (25b)$$

where

$$r_{pq} = \frac{n_p - n_q}{n_p + n_q} \quad (26a)$$

$$t_{pq} = \frac{2n_p}{n_p + n_q}, \quad (26b)$$

are the reflection and transmission coefficients corresponding to a single interface separating medium p from medium q ($p, q = i, \mu, t$), d is the film thickness, and $k_\mu = (\omega/c)n_\mu$ is the wavenumber within the film corresponding to the mode $\mu = 1, 2$.

According to Eq. (23), the reflected and transmitted electric fields are given by

$$\mathbf{E}_r = \sum_\mu r_\mu \mathbf{E}_i \cdot \tilde{\mathbf{V}}_\mu \mathbf{V}_\mu, \quad (27a)$$

$$\mathbf{E}_t = \sum_\mu t_\mu \mathbf{E}_i \cdot \tilde{\mathbf{V}}_\mu \mathbf{V}_\mu. \quad (27b)$$

The reflectance and transmittance are given by

$$R = \frac{|\mathbf{E}_r|^2}{|\mathbf{E}_i|^2}, \quad (28a)$$

$$T = \frac{n_t}{n_i} \frac{|\mathbf{E}_t|^2}{|\mathbf{E}_i|^2}, \quad (28b)$$

and the polarization properties of the incident, reflected and transmitted field may be found through the analysis of subsection II B.

The optical properties obtained above depend implicitly on the frequency of the incident field through n_μ , which inherits its frequency dependence from the response $\epsilon_a(\omega)$ and $\epsilon_b(\omega)$ of the components A and B of the metamaterial.

D. Polarization

We can write Eqs. (27) as a matrix equation

$$\mathbf{E}_\alpha = \mathbf{J}_\alpha \cdot \mathbf{E}_i, \quad (\alpha = t, r), \quad (29)$$

where

$$\mathbf{J}_\alpha = \begin{pmatrix} V_{x1} & V_{x2} \\ V_{y1} & V_{y2} \end{pmatrix} \begin{pmatrix} \alpha_1 & 0 \\ 0 & \alpha_2 \end{pmatrix} \begin{pmatrix} \tilde{V}_{1x} & \tilde{V}_{1y} \\ \tilde{V}_{2x} & \tilde{V}_{2y} \end{pmatrix} \quad (30)$$

denote the Jones matrices³⁹ for reflection ($\alpha = r$) or transmission ($\alpha = t$), and where r_μ and t_μ ($\mu = 1, 2$) are taken from Eqs. (25). The Jones matrices (30) allow us to calculate the polarization of the reflected and transmitted light from the polarization of the incoming wave, assumed to be in a pure polarized state. When the incoming wave is not in a pure state but has an unpolarized component, we can describe its polarization state in terms of the Stokes vectors \mathbf{S}_α for the reflected ($\alpha = r$) and the transmitted ($\alpha = t$) wave, which are related to the incoming polarization state \mathbf{S}_i through

$$\mathbf{S}_\alpha = \mathbf{M}_\alpha \cdot \mathbf{S}_i, \quad (\alpha = r, t). \quad (31)$$

in terms of the Mueller matrices \mathbf{M}_α , with components³⁹

$$m_{ij}^\alpha = \frac{1}{2} \text{Tr}(\mathbf{J}_\alpha \sigma_i \mathbf{J}_\alpha^\dagger \sigma_j), \quad (\alpha = t, r), \quad (i, j = 0, 1, 2, 3), \quad (32)$$

with σ_i the Pauli matrices plus the identity, i.e.

$$\sigma_0 = \begin{pmatrix} 1 & 0 \\ 0 & 1 \end{pmatrix} \quad \sigma_1 = \begin{pmatrix} 1 & 0 \\ 0 & -1 \end{pmatrix} \quad \sigma_2 = \begin{pmatrix} 0 & 1 \\ 1 & 0 \end{pmatrix} \quad \sigma_3 = \begin{pmatrix} 0 & -i \\ i & 0 \end{pmatrix}, \quad (33)$$

and where J_α^\dagger denotes the adjunct of the matrix J_α . For example, for unpolarized (natural) incoming light, the input Stokes vector would be

$$\mathbf{S}_i = (1, 0, 0, 0)^T, \quad (34)$$

so the output Stokes vector would be

$$\mathbf{S}_\alpha = (m_{00}^\alpha, m_{10}^\alpha, m_{20}^\alpha, m_{30}^\alpha)^T, \quad (\alpha = r, t). \quad (35)$$

Here, the superscript T denotes transpose.

The degree of polarization of the outgoing waves can be described by

$$P_\alpha = \frac{(S_{\alpha 1}^2 + S_{\alpha 2}^2 + S_{\alpha 3}^2)^{1/2}}{S_{\alpha 0}} \leq 1; \quad (36)$$

$P_\alpha = 1$ corresponds to fully polarized and $P_\alpha = 0$ corresponds to unpolarized light. The kind of full or partial polarization may be read from the Stokes coefficients: $S_{\alpha 1} > 0$ corresponds to (partial) linear horizontal polarization while $S_{\alpha 1} < 0$ corresponds to vertical polarization, $S_{\alpha 2} > 0$ to polarization along 45° from the x towards the y axis, while $S_{\alpha 2} < 0$ corresponds to 135° , $S_{\alpha 3} > 0$ corresponds to circular right-handed polarization, and $S_{\alpha 3} < 0$ to circular left-handed polarization.

III. RESULTS

We first consider a metamaterial made out of a thin conducting film of width d deposited on an isotropic dielectric substrate with index of refraction n_t and with a square array of holes ($\epsilon_b = 1$) in the form of crosses, as those shown in Fig. 1. The geometry of the system is then characterized by the lengths L_x and L_y of the beams of the cross along the x and y directions, their widths W_x and W_y and the angle ϕ between one beam of the cross and the x axis. We can tune these parameters to design systems with desired optical properties.

In Fig. 2 we show the transmittance and reflectance T and R of a silver film ($\epsilon_a = \epsilon_{\text{Ag}}$) of width $d = 100$ nm deposited over glass ($n_t = 1.4$) with a square array of cross-shaped holes aligned with the lattice axes $\phi = 0$ with geometry characterized by $L_x = 0.965a$, $L_y = 0.848a$, $W_x = 0.299a$, and $W_y = 0.374a$, where a is the lattice parameter. We show results for normally incident linearly polarized incoming light,

$$\mathbf{E}_i = E_{oi}(\cos \theta, \sin \theta), \quad (37)$$

with θ the angle of polarization with respect to the X direction. We display results for polarization along the X -axis ($\theta = 0$) and along the Y -axis ($\theta = 90^\circ$). We performed this and the following calculations using the recursive methods developed in Ref. 22 within a lattice of 601×601 pixels and using between 200 and 400 Haydock's coefficients. The programs were developed using the Perl Data Language (PDL).^{40,41}

In this system, X and Y are symmetry directions, and therefore they coincide with the principal directions of the macroscopic response. Thus, for input polarization angles $\theta = 0, 90^\circ$ the outgoing polarizations coincide with the

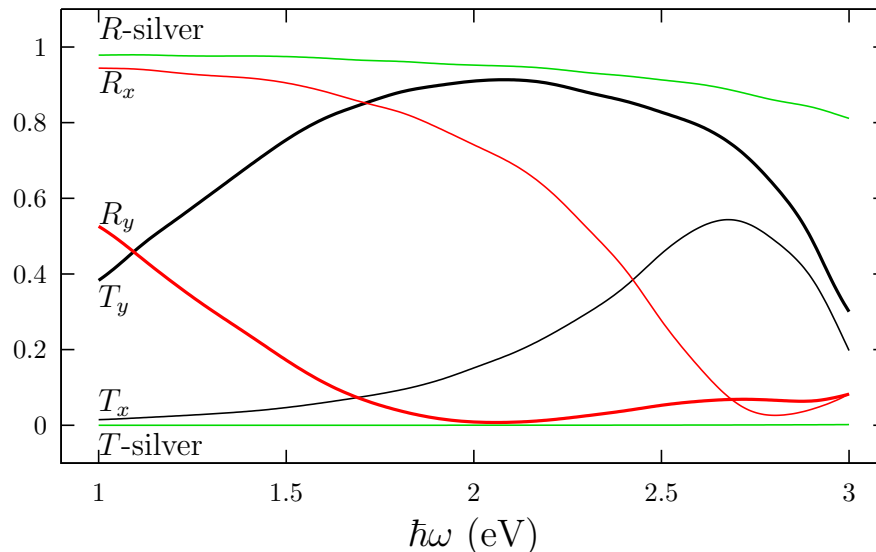


FIG. 2: Normal incidence reflectance R_μ and transmittance T_μ ($\mu = x, y$) of a $d = 100$ nm Ag film on glass with a subwavelength square array of cross shaped holes with $L_x = 0.965a$, $L_y = 0.848a$, $W_x = 0.299a$, and $W_y = 0.374a$, with a the lattice parameter, for an incident wave linearly polarized along X and Y directions as a function of photon energy. Also shown are the reflectance and transmittance for a uniform Ag film of width $d = 50$ nm and thus, with the same amount of metal.

incoming polarizations. Notice that there is a sizable energy range around 2eV for which R_y is below 1% and T_y is above 80%, while, rotating the incoming polarization by 90° , R_x becomes much larger than T_x . Thus, this system displays a very large linear dichroism both under transmission and under reflection. The reason for this behavior is the extraordinary transmission present in conducting films whenever the conducting paths are almost choked, and is due to the matching between the vacuum surface impedance and the surface impedance of the film as it transits from being conductor-like at low frequencies and dielectric-like at high frequencies.^{20,42} Notice that for this system, $P_x = 0.035a$ and $P_y = 0.152a$, so it has relatively wide conducting paths along the x direction, but very narrow passages along the y direction. Therefore, the film displays extraordinary transmission for y polarization but is opaque and thus has a large reflectance for x polarization. Thus, its extreme dichroism. For comparison purposes, in the same figure we have plotted the transmittance of a much thinner flat homogeneous Ag film, of width $d = 50$ nm chosen so both films contain the same amount of silver. We remark that the transmittance T_y for y polarization is about three orders of magnitude larger than that of the homogeneous film, although the latter is narrower.

In Fig. 3 we show the normal incidence transmittance and reflectance T and R of a system with $L_x = 0.963a$, $L_y = a$, $W_x = 0.249a$ and $W_y = 0.324a$. In contrast to the previous case, conducting paths along x are completely closed instead of being wide open as in Fig. 2. The conducting paths along y are almost blocked, as $P_x = 0.07a$. In this case, the system behaves as an anisotropic insulator unless the frequency is low enough that the response along y becomes conductor-like. The frequency of this dielectric-conductor change of behavior may be tuned by changing the width P_x of the narrow channels. The reflectance and transmittance and the polarization of the outgoing light depend on the input polarization. The results displayed in Fig. 3 correspond to incoming light that is linearly polarized at an angle $\theta = 45^\circ$ with respect to the x -axis. In the same figure we indicated the shape of the polarization ellipses corresponding to the outgoing waves and we color coded their helicity. Notice that for a very wide frequency range we were able to obtain right handed almost circularly polarized transmitted light with a transmittance T above 70%. Given the geometrical symmetry of this system, as the incoming polarization angle θ diminishes towards 0 or increases towards 90° the outgoing polarization becomes linear, and as θ approaches -45° we obtain again circularly polarized light but with the opposite helicity. Thus our system behaves as a quarter-wave plate, though it is of subwavelength thickness and is operational over a wide frequency range.

In Fig. 4 we show the third flattening η_t that characterizes the degree of circular polarization of the transmitted fields corresponding to the same system as in Fig. 3, for incident light linearly polarized along $\theta = 45^\circ$ or 135° . The film is wider $d = 140$ nm and the holes are filled with a transparent material with dielectric constant ϵ_b . We notice the wide energy regions for which η_T is close to zero (say, < 0.1) and the fact that these regions may be shifted by changing the dielectric constant ϵ_b of the insulating material. We have verified that the results above remain valid qualitatively under changes of the geometrical parameters, although the angle of the incoming polarization to obtain

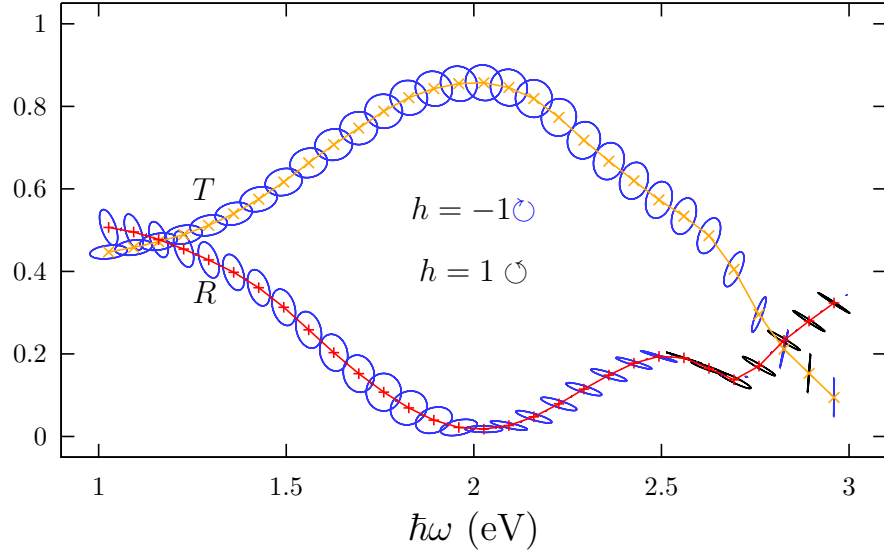


FIG. 3: Normal incidence reflectance R and transmittance T for the same system as in Fig. 2 but with $L_x = 0.963a$, $L_y = a$, $W_x = 0.249a$ and $W_y = 0.324a$ as a function of the photon energy. The incoming wave is linearly polarized with $\theta = 45^\circ$. We indicate the polarization ellipses of the outgoing waves and we color code their helicities.

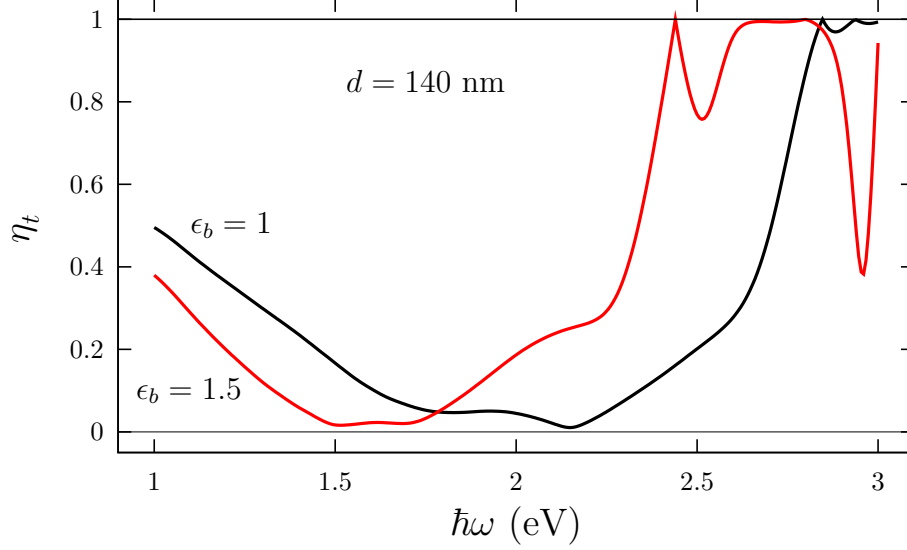


FIG. 4: Third flattening η_t for the transmitted fields corresponding to Fig. 3 illuminated by a field that is linearly polarized at $\theta = 45^\circ$ or 135° . The film has a width $d = 140$ nm and its holes are filled with an insulator with dielectric constant ϵ_b .

circular polarization might have to be adjusted away from 45° , 135° , and the energy range for which we obtain circular polarization may also change.

In Fig. 5 we show the third flattening η_t and the transmittance T for light transmitted through a film as in Fig. 4 but of different widths $d = 80, 90, \dots, 140$ nm when illuminated by light linearly polarized along $\theta = 35^\circ$ or 145° . The holes in the Ag film are filled with an insulator with dielectric constant $\epsilon_b = 1.5$. Notice that fully circular polarization ($\eta_t = 0$) is achieved at a frequency that may be shifted by 0.3 eV by changing the width of the film. The black dots in the lower panel show that the transmittance is appreciable ($T > 0.3$) at those frequencies for which the transmitted field is completely circularly polarized. Similar results hold for other dielectrics and other polarization angles and it is possible to design the system to produce circularly polarized light at any visible frequency.

The systems analyzed above are symmetric under $x \rightarrow -x$ and $y \rightarrow -y$ reflections, and therefore, they display no circular dichroism and they yield no circular polarization when illuminated by natural, unpolarized light. Thus, to

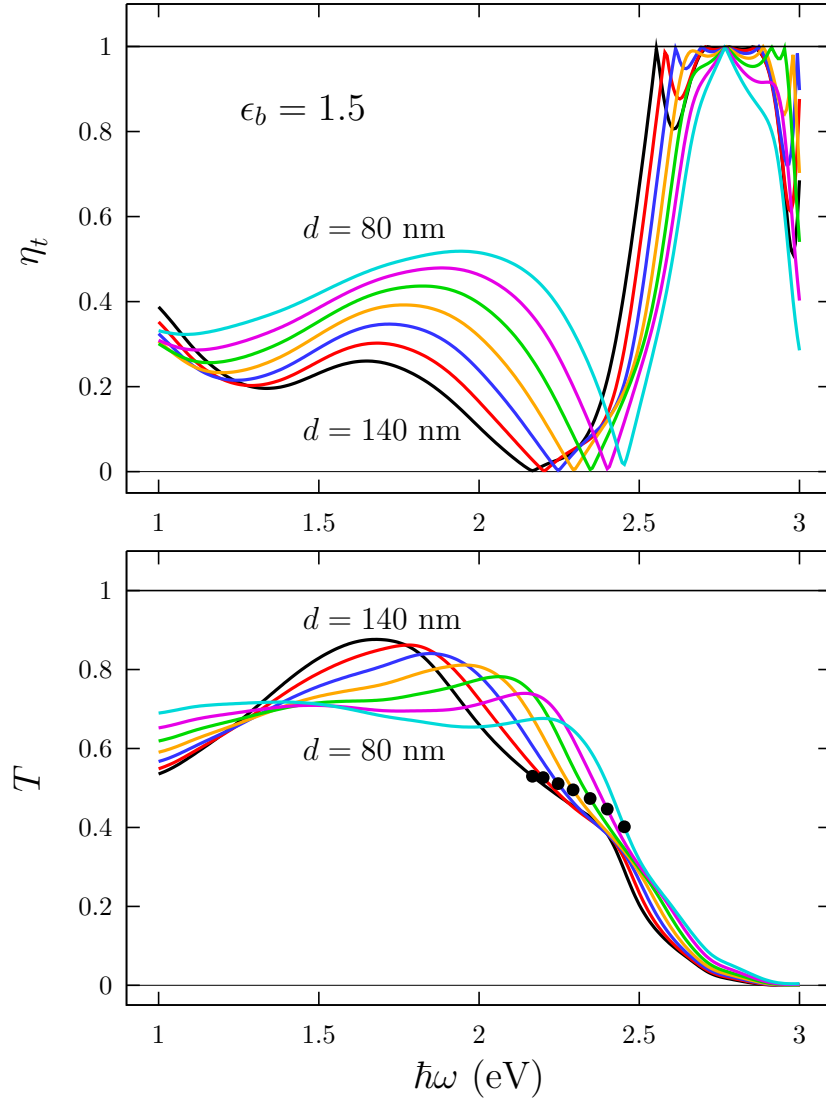


FIG. 5: Third flattening η_t (upper panel) for the transmitted light and transmittance T (lower panel) for the same film as in Fig. 4 with the holes filled by an insulator with dielectric constant $\epsilon_b = 1.5$ and for different film widths $d = 80, 90 \dots 140$ nm, when illuminated by light linearly polarized along $\theta = 35^\circ, 145^\circ$. The black dots in the lower panel correspond to the crossings $\eta_t = 0$ in the upper panel.

explore metamaterials with circular dichroism and circular polarizers, we now consider a system that has no in-plane reflection symmetry.

In Fig. 6 we show one such system, consisting of an Ag film deposited on a glass substrate and from which a square lattice of pairs of holes have been carved out and filled with a dielectric. The holes have the shape of prisms characterized by their width W and height H , and relative displacement ρ between pairs of holes within each cell besides the width d of the film and the dielectric function ϵ_b of the inclusions. We optimized these parameters, as well as the width d of the film and the dielectric constant ϵ_b of the inclusions in order to maximize the sought optical properties of the film. Notice that for some values of the parameters, the dielectric filled holes might overlap each other; our calculation procedure is able to cope with such situations.

In Fig. 7 we show the degree of circular polarization $\mathcal{C}_t \equiv S_{t3}/S_{t0}$, of light transmitted through a $d = 100$ nm Ag and dielectric metamaterial film on glass, as in Fig. 6, when illuminated by unpolarized light, corresponding to $S_i = (1, 0, 0, 0)$. We show results for given values of the dielectric constant $\epsilon_b = 2, 3, 5$ and the geometrical parameters, given in table I, were obtained by finding the maximum circularity within the visible range and optimizing it. Thus, at each step during the optimization procedure we calculated the full spectra for each set of candidate parameters. To guarantee a not-too-low transmittance, we actually maximized a mixture of the degree of circular polarization \mathcal{C}_t ,

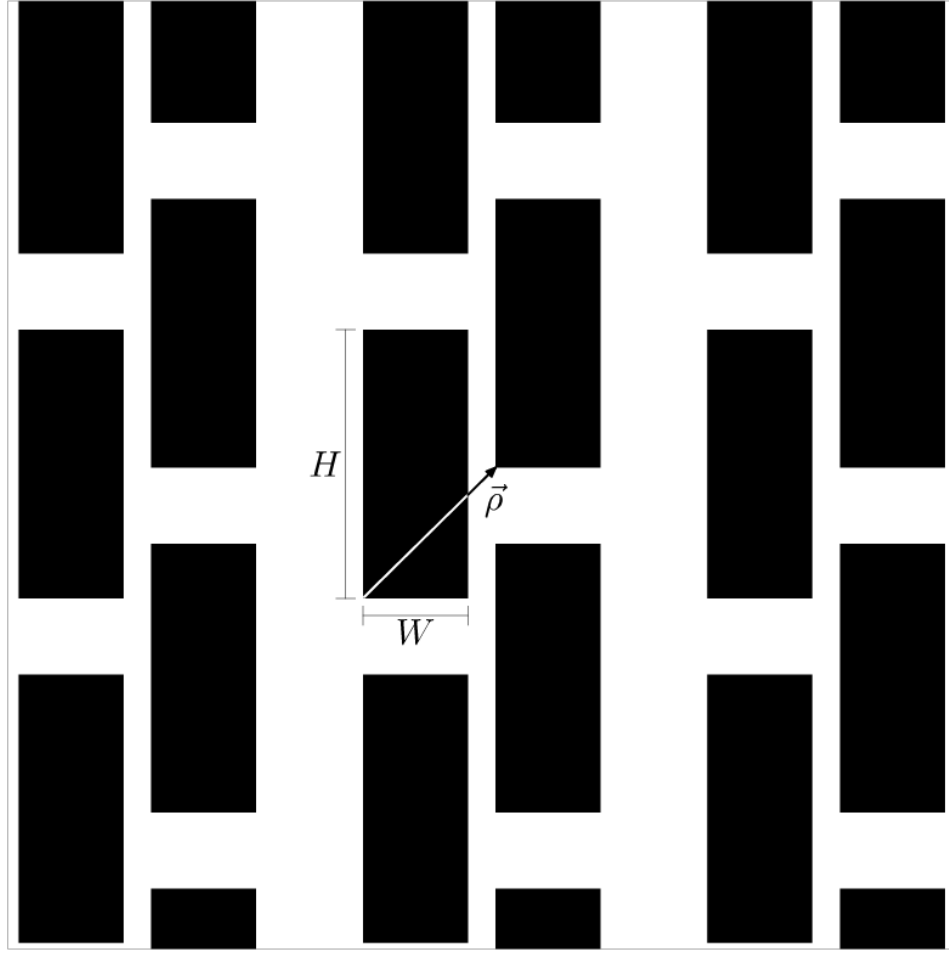


FIG. 6: Ag film (white) deposited on a glass substrate and from which a square lattice of pairs of holes in the shape of rectangular prisms have been carved out and filled with a dielectric (black). The geometry is characterized by the width W and height H of the prisms and the relative displacement ρ between pairs of holes within the unit cell. For some values of these parameters the dielectric filled holes might overlap each other.

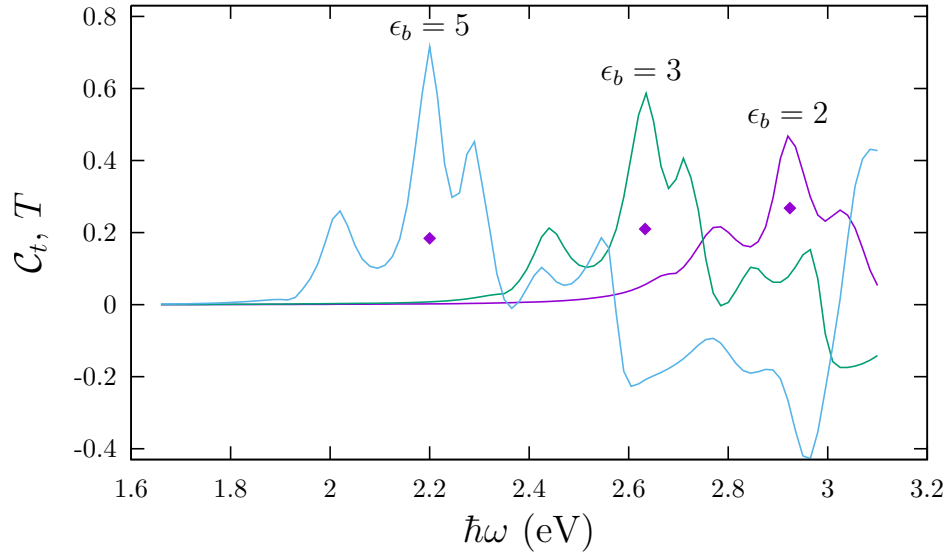


FIG. 7: Degree of circular polarization C_t of light transmitted through a $d = 100$ nm Ag film with a geometry as shown in Fig. 6 with parameters given in table I when illuminated by unpolarized light $S_i = (1, 0, 0, 0)$. We display with solid circles the maxima of C_t and with solid diamonds the corresponding transmittance T .

ϵ_b	W/a	H/a	ρ_x/a	ρ_y/a
2	0.305	0.732	0.383	-0.304
3	0.305	0.777	0.385	-0.379
5	0.305	0.779	0.385	-0.379

TABLE I: Optimized geometrical parameters of the system shown in Fig. 6 to produce the largest circular polarization \mathcal{C}_t within the visible range (see Fig. 7) with a large enough transmittance T for various values of the dielectric constant $\epsilon_b = 2, 3, 5$ for a film of thickness $d = 100$ nm. over a glass substrate. The distances are expressed as fractions of the lattice parameter a .

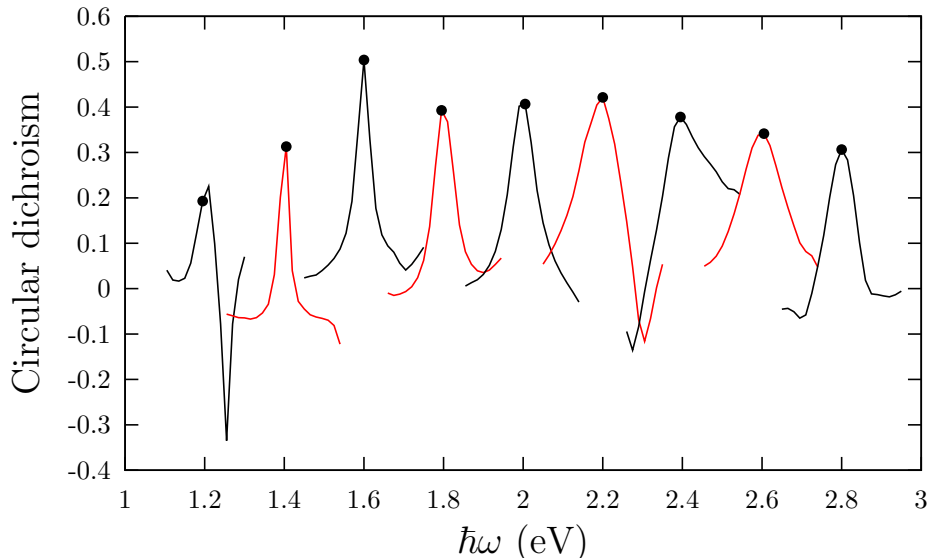


FIG. 8: Circular dichroism CD of a series of films with the geometry described by Fig. 6 and the parameters shown in table II. We only show part of the spectra around the energies $\hbar\omega_0$ for which the parameters were optimized, and we indicate with the solid dots the corresponding optimized values $CD(\omega_0)$.

and the transmittance $T = S_{t0}$, to wit, the product of two sigmoidal functions of width 0.1 evaluated at \mathcal{C}_t and at T , and centered at 0.8 and 0.2, respectively. As illustrated in Fig. 7, the degree of circular polarization may attain peaks with $\mathcal{C}_t = 0.7$ or even higher, with a corresponding transmittance larger than ≈ 0.2 , and these peaks may be tuned within the whole visible range by adequately choosing the value of the dielectric constant ϵ_b . We remark that our computational scheme is fast enough to allow the calculation of the full spectra *at each step* of the optimization process. We performed the optimizations using the simplex method offered by the MINUIT package developed at CERN⁴³ and its PDL^{40,41} interface.⁴⁴

Instead of searching for a maximum within a range of frequencies, we can search for a maximum of any desired optical property at given desired frequencies. To illustrate this case, in Fig. 8 we show the circular dichroism $CD = \mathcal{A}_L - \mathcal{A}_R$ of a set of films with the geometrical parameters, as well as the dielectric constants ϵ_b and the thickness d of the film, obtained by optimizing CD at chosen frequencies $\hbar\omega_0 = 1.2$ eV, 1.4 eV...2.8 eV and given in table II. Here, \mathcal{A}_L (\mathcal{A}_R) is the absorbance of the film corresponding to left-handed (right-handed) circularly polarized incident light.

Notice that with our simple geometry we obtained a circular dichroism that peaks at our chosen frequencies which we tuned across the near infrared and the visible region. Its maximum values are larger than 0.2 and as large as 0.5, much larger than those of naturally occurring chiral materials, although our system is a thin film, its texture has subwavelength characteristic distances, its geometry is not chiral³² and the incoming light is normally incident.⁴⁵

IV. CONCLUSIONS

We employed Haydock's recursive method within the long wavelength approximation to calculate the complex frequency dependent macroscopic dielectric tensor ϵ_M^{ij} of metamaterials in terms of the dielectric functions of the host ϵ_a and the inclusions ϵ_b , and of the geometry of both the unit cell and the inclusions. The calculation requires modest computing resources to obtain well converged results which can be applied to metamaterials with dispersive and dissipative as well as transparent components. The input to our calculations are images of the unit cells which

$\hbar\omega_0$ (eV)	W/a	H/a	ρ_x/a	ρ_y/a	ϵ_b	d (nm)
1.2	0.491	0.815	0.499	-0.147	6.635	200
1.4	0.490	0.793	0.461	-0.140	6.625	200
1.6	0.415	0.652	0.434	0.191	6.939	171
1.8	0.500	0.677	0.452	-0.214	4.893	198
2.0	0.472	0.870	0.451	-0.213	4.842	166
2.2	0.478	0.874	0.462	0.220	5.390	172
2.4	0.485	0.844	0.483	0.282	5.470	172
2.6	0.490	0.827	0.473	0.297	5.178	175
2.8	0.470	0.788	0.481	-0.302	5.465	177

TABLE II: Parameters (width W , height H , displacement (ρ_x, ρ_y) , dielectric constant ϵ_b and film thickness d) that optimize at the chosen frequency ω_0 the circular dichroism of an Ag film with dielectric inclusions. The geometry and the parameters are as in Fig. 6.

may be manipulated using image processing software, thus allowing us to rapidly explore manifold geometries in a design process to obtain a tailored optical response.

We found that a simple system made up of a square array of cross-shaped nanometric holes with slightly anisotropic geometrical properties carved out of a thin supported silver film may display a very strong linear dichroic response for both transmission and reflection. Rotating the direction of polarization of the incoming wave, the transmittance of the system could change from the very small value expected of homogeneous Ag films to an extraordinary transmittance that is about three orders of magnitude larger. Furthermore, the same system but with different geometrical parameters behaves as a quarter wave plate, producing circularly polarized output light for a linearly polarized input field with an helicity that can be controlled by rotating the input polarization direction, although the width of the film is much thinner than the wavelength. Moreover, this behavior may be tuned over a wide frequency range that covers the visible spectrum.

We also explored systems with no reflection symmetry within the surface of the film and we were able to tune the parameters in order to optimize different optical properties related to the circular polarization of light. Thus, we obtained that a thin Ag film crossed by a lattice of appropriately patterned insulating regions could behave as a circular polarizer, yielding circularly polarized light when illuminated by unpolarized light, with peak degrees of circular polarization above 0.7, and that a similar system with different parameters yielded a film with extreme circular dichroism as large as 0.5, much higher than that of naturally occurring chiral materials. We remark that our system is a thin film, its texture has subwavelength characteristic distances, its geometry is not chiral and the incoming light is normally incident.

These examples illustrate how standard optical elements may be replaced by thin nanometric patterned films with the same or better performance, which may thus be integrated into nano-photonic devices. The design of these elements benefit greatly from the availability of our very efficient computational procedure, which allowed us to optimize the geometrical parameters of the system.

Acknowledgments

We acknowledge partial support from DGAPA-UNAM through grant IN113016 (WLM) and from CONACyT 153930 (BSM). We are grateful to J. Samuel Pérez-Huerta and Guillermo Ortiz for useful discussions.

-
- ¹ J.C.Garland and D.B.Tanner, eds., *Electrical Transport and Optical Properties of Inhomogeneous Media*, AIP Conference Proceeding No. 40 (American Institute of Physics, New York, 1978).
 - ² W. Mochán and R. Barrera, eds., *Electrical Transport and Optical Properties of Inhomogeneous Media*, vol. 207 (1-3) of *Physica A* (Elsevier, The Netherlands, 1994).
 - ³ G. Milton, K. Golden, D. Dobson, and A. Vardeny, eds., *Electrical Transport and Optical Properties of Inhomogeneous Media*, vol. 338 of *Physica B* (Elsevier, North-Holland, 2003).
 - ⁴ Y. Akahane, T. Asano, B.-S. Song, and S. Noda, *Nature* **425**, 944 (2003).
 - ⁵ A. N. Grigorenko, A. K. Geim, H. F. Gleeson, Y. Zhang, A. A. Firsov, I. Y. Khrushchev, and J. Petrovic, *Nature* **438**, 335 (2005).

- ⁶ K. K. Koerkamp, S. Enoch, F. B. Segerink, N. van Hulst, and L. Kuipers, Phys. Rev. Lett. **92**, 183901 (2004).
- ⁷ R. Gordon, A. G. Brolo, A. McKinnon, A. Rajora, B. Leathem, and K. L. Kavanagh, Phys. Rev. Lett. **92**, 037401 (2004).
- ⁸ J. Pendry, Phys. Rev. Lett. **85**, 3966 (2000).
- ⁹ V. Shalaev, W. Cat, U. Chettiar, H. Yuan, A. Sarychev, V. Drachev, and A. Kildishev, Opt. Lett. **30**, 3356 (2005).
- ¹⁰ A. Kildishev, W. Cai, U. Chettiar, H.-K. Yuan, A. Sarychev, V. P. Drachev, and V. M. Shalaev, J. Opt. Soc. Am. B **23**, 423 (2006).
- ¹¹ U. Leonhardt, Science **312**, 1777 (2006).
- ¹² J. B. Pendry, D. Schurig, and D. R. Smith, Science **312**, 1780 (2006), URL [DOI:10.1126/science.1125907](https://doi.org/10.1126/science.1125907).
- ¹³ G. W. Milton and N.-A. P. Nicorovici, Proceedings of the Royal Society A **462**, 3027 (2006), URL <http://rspa.royalsocietypublishing.org/content/462/2074/3027>.
- ¹⁴ S. Feng and K. Halterman, Phys. Rev. Lett. **100**, 063901 (2008), URL <http://journals.aps.org/prl/abstract/10.1103/PhysRevLett.100.063901>.
- ¹⁵ Z. Liu, H. Lee, Y. Xiong, C. Sun, and X. Zhang, Science **315**, 1686 (2007).
- ¹⁶ W. L. Barnes, A. Dereux, and T. W. Ebbesen, Nature **424**, 824 (2003), URL [doi:10.1038/nature01937](https://doi.org/10.1038/nature01937).
- ¹⁷ J. Lin, J. B. Mueller, Q. Wang, G. Yuan, N. Antoniou, X.-C. Yuan, and F. Capasso, Science **340**, 331 (2013).
- ¹⁸ Y. Cui, L. Kang, S. Lan, S. Rodrigues, and W. Cai, Nano Letters **14**, 1021 (2014), URL [doi:10.1021/nl404572u](https://doi.org/10.1021/nl404572u).
- ¹⁹ W. Li, Z. J. Coppens, L. V. Besteiro, W. Wang, A. O. Govorov, and J. Valentine, Nature Communications **6**, 8379 (2015), URL [doi:10.1038/ncomms9379](https://doi.org/10.1038/ncomms9379).
- ²⁰ B. S. Mendoza and W. L. Mochán, Phys. Rev. B **85**, 125418 (2012), URL <http://link.aps.org/doi/10.1103/PhysRevB.85.125418>.
- ²¹ R. Haydock, Solid State Physics **35**, 215 (1980).
- ²² W. L. Mochán, G. P. Ortiz, and B. S. Mendoza, Opt. Express **18**, 22119 (2010).
- ²³ E. Cortés, W. L. Mochán, B. S. Mendoza, and G. P. Ortiz, Phys. Status Solidi B **247**, 2102 (2010).
- ²⁴ G. P. Ortiz, B. E. Martínez-Zérega, B. S. Mendoza, and W. L. Mochán, Phys. Rev. B **109**, 245132 (2009).
- ²⁵ W. Mochán and R. Barrera, Phys. Rev. B **32**, 4984 (1985).
- ²⁶ P. Halevi and F. Pérez-Rodríguez, SPIE **6320** (2006).
- ²⁷ A. Krokhin, P. Halevi, and J. Arriaga, Phys. Rev. B **65**, 115208 (2002).
- ²⁸ P. Halevi, A. Krokhin, and J. Arriaga, Phys. Rev. Lett. **82**, 719 (1999).
- ²⁹ S. Datta, C. T. Chan, K. M. Ho, and C. M. Soukoulis, Phys. Rev. B **48**, 14936 (1993).
- ³⁰ S. Zhang, Y.-S. Park, J. Li, X. Lu, W. Zhang, and X. Zhang, Phys. Rev. Lett. **102**, 023901 (2009).
- ³¹ X. Xiong, W.-H. Sun, Y.-J. Bao, M. Wang, R.-W. Peng, C. Sun, X. Lu, J. Shao, Z.-F. Li, and N.-B. Ming, Phys. Rev. B **81**, 075119 (2010).
- ³² J. Kaschke, L. Blume, L. Wu, M. Thiel, K. Bade, Z. Yang, and M. Wegener, Advanced Optical Materials **3**, 1411 (2015), URL [doi:10.1002/adom.201500194](https://doi.org/10.1002/adom.201500194).
- ³³ J. S. Pérez-Huerta, G. P. Ortiz, B. S. Mendoza, and W. Luis Mochán, New Journal of Physics **15**, 043037 (2013), ISSN 1367-2630, URL <http://stacks.iop.org/1367-2630/15/i=4/a=043037?key=crossref.a59a111da6634ef4e693f1d2d8edebe3>.
- ³⁴ Y.-H. Wang, J. Shao, J. Li, M.-J. Zhu, J. Li, L. Zhou, and Z.-G. Dong, Journal of Physics D-Applied Physics **48**, 485306 (2015), URL [doi:10.1088/0022-3727/48/48/485306](https://doi.org/10.1088/0022-3727/48/48/485306).
- ³⁵ Since the long-wavelength response ϵ_M is independent of the direction of $\mathbf{q} \rightarrow 0$, one can use the results of the longitudinal calculations to solve optical (transverse) problems.
- ³⁶ R. Barrera, A. Reyes-Coronado, and A. García-Valenzuela, Phys. Rev. B **75**, 184202 (2007).
- ³⁷ M. Born and E. Wolf, *Principles of Optics* (Cambridge University Press, Cambridge, 1999), 7th ed.
- ³⁸ G. Arfken, *Mathematical Methods for Physicist* (Academic Press, New York, 1970), chap. 4, 2nd ed.
- ³⁹ C. Brosseau, *Fundamentals of Polarized Light* (John Wiley and Sons, Inc., New York, 1988).
- ⁴⁰ K. Glazebrook and F. Economou, *Pdl: The perl data language*, Dr. Dobb's Journal, URL <http://www.ddj.com/184410442>.
- ⁴¹ K. Glazebrook and J. Brinchmann and J. Cerney and C. DeForest and D. Hunt and T. Jenness and T. Luka and R. Schwebel and C. Soeller, *The perl data language v2.4.4*, URL <http://pdl.perl.org>.
- ⁴² B. S. Mendoza and W. L. Mochán, Phys. Rev. B **85**, 125418 (2012).
- ⁴³ F. James, *Minuit – Function Minimization and Error Analysis Reference Manual*, CERN, Geneva, 94th ed. (1994), URL <http://hep.fi.infn.it/minuit.pdf>.
- ⁴⁴ A. Jordan, *PDL::Minuit – a PDL interface to the Minuit library* (2007), URL <http://search.cpan.org/~chm/PDL-2.015/GENERATED/PDL/Minuit.pm>.
- ⁴⁵ T. Cao, C. Wei, and L. Mao, Scientific Reports **5**, 14666 (2015), URL [doi:10.1038/srep14666](https://doi.org/10.1038/srep14666).